Final report

Chao Wang, M.Sc.

chao.wang@stud.unileoben.ac.at

Montanuniversität Leoben, Austria

Supervisors at home university:

- **Prof. Gerald Pinter,** gerald.pinter@unileoben.ac.at
- **Prof. Florian Grün,** florian.gruen@unileoben.ac.at
- **Montanuniversität Leoben, Austria**

Supervisor at guest university:

- **Prof. Alison Dunn,** acd@illinois.edu
- **University of Illinois at Urbana-Champaign, USA**

March. 2019

Contents

Title: Investigation of the local friction and wear process of sealing materials by means of in situ technique

1. Introduction

With the development of technology, seals are playing a more and more critical role in modern machines. At the same time, higher requirements on seals were expected. In order to achieve these requirements, scientists have developed new materials, novel structures, and lubricants (Nikas 2016). The mechanical seals are designed to provide flat radial faces, one of them is in contact with rotary surface. Its function is to contain fluid in a closed area and prevent the leakage of fluid from machine and keep contaminations out of the machine, such as centrifugal pumps, rotary compressors.

Elastomers have several advantages, which make them widely used in a variety of applications as sealing materials. Their low Young's modulus, low shear modulus, and high failure strain make them as ideal materials to deform largely and fit in special geometries. In addition, their incompressibility, which results from their high Poisson's ratio (close to 0.5) make it possible, to transfer applied pressure without change their volume. However, their disadvantages can bring severe problems, if they are used incorrectly or in a wrong application. The American Space Shuttle Challenger disaster occurred on January 28, 1986. The shuttle exploded after lunch, which was caused by the failure of O-ring seals used in the joint that were not designed to handle the unusually cold conditions that existed at this launch (Redesigning the space shuttles solid rocket motor seals 1996). Their mechanical properties change extremely. If the temperature is below a critical temperature, which is called the glass transition temperature (Tg), the materials change from rubber-like materials to glass. Furthermore, their tribological properties are not always predictable.

The failures of seals can be resulted from various mechanisms, e.g. incorrect shaft manufacture, incorrect assembly, a faulty seal, lubricant incompatibility, excessively high temperatures, vibration, or dirt, etc. (Flitney 2014). Stick-slip problem can be caused by insufficient lubrication at low speed and high pressure, e.g. running -in phase. Thus, understanding the mechanism of stick-slip and the local friction process of sealing materials is of great importance.

1.1. Friction and wear of elastomeric seals

Due to its special material properties, two main mechanisms are responsible for the friction between elastomers and hard surfaces (Grosch 1963). Adhesion is generally recognized to consist in making and breaking the molecular bonding (Moore and Geyer 1972; Belyi et al. 1977); (Zeng 2013; Myshkin et al. 2005; Johnson 1997; Maeda et al. 2002). The low elasticity of elastomers leads to large deformation under normal stress, which results in energy loss associated with internal damping effects within a viscoelastic body. The lost energy is normally transformed in heat. Depends on the material properties, under unlubricated conditions, adhesion generally is the dominant friction factor (Moore and Geyer 1974; Heinrich 1997; Zhang 2004). The hysteresis factor can be negligible. However, under lubricated conditions, the adhesive part is reduced significantly, and the hysteresis part keeps almost constant. Thus, the hysteresis part plays an important role under lubricated conditions.

Schallamach (Schallamach 1971) and Johnson (Johnson et al. 1971) have made a considerable progress in understanding of rubber friction behavior. Schallamach has observed the contact area, when a hard slider slides on a rubber surface. He observed the "wave of detachment", which was known as Schallamach waves. They are cross the contact area at high speed from front to rear of the slider. Adhesion appears to be complete between these waves which are moving folds in the rubber surface. Each fold creates a ridge in which air is trapped and as the fold passes though the contact region the surface contact is broken locally as the rubber surface is lifted out of contact. Fukahori (Fukahori et al. 2010) has introduced two new insights to elucidate the mechanism of the initiation and propagation of the wave of detachment, firstly the surface interaction force can produce a meniscus effect at the rubber surface and secondly the stick–slip motion can be seen to have a significant role during the sliding of rubber. They revealed that the meniscus developed on the rubber surface allows a wave of detachment to be formed at the leading edge of contact due to the compression stress field. At the trailing edge a ripple is formed due to the tensile stress field. The initial slow propagation of the wave is governed by the compressive stress field and the location where the fold is formed. The increase in wave propagation velocity is closely related to the slipping process in stick–slip motion and thus the characteristics in propagation of the waves such as the periodicity, the high velocity and the sliding velocity dependence all correlate well to the periodic stick–slip motion. True sliding must take place with or without Schallamach waves. The contribution of Schallamach waves to the frictional sliding of rubber is to make the contact area smaller periodically, and thus yield a smoother sliding with smaller stick–slip motion during

rubber friction. The waves always originate at the leading edge of the contact and move to the trailing edge. The wave moves slightly faster than sliding velocity at the initial frontal zone, but increases in velocity (much more than tenfold of sliding velocity) at around the center of the whole contact after passing the front region (Barquins and Courtel 1975; Uchiyama 1985).

In the study of Johnson et al. (Johnson et al. 1971), They revealed that the area of contact between a rigid sphere and a flat rubber surface was larger than the value estimated from the Hertzian contact theory. They proposed that the molecular attraction of van der Waals forces, acting between the sphere and the rubber surface, lead to an increase in the contact area.

As to wear, abrasive, adhesive and fatigue wear are the three main wear mechanisms for elastomer (Myshkin et al. 2005). Abrasive wear is caused by sharp asperities of the hard counterpart as a result of tearing of the sliding surface of the elastomer. Fatigue wear is a kind of wear mechanism, which occurs on the surface of an elastomer sliding resulting in a change in the material state due to repeated (cyclic) stressing which results in progressive fracture. It is characterized by the accumulation of irreversible changes that lead to generation and further development of cracks. The loss of material from solid surfaces due to frictional fatigue is referred to as fatigue wear. As a result, two different stress fields are developed in surface and sub-surface areas with different scales of the diameter, the apparent contact area on the surface, and the local contact point in the sub-surface region. These regions are responsible for material fatigue in these areas responsible for the generation and propagation of cracks and the formation of wear particles. When a highly elastic elastomer slides against a smooth surface, roll formation occurs. In this type of wear the high frictional force shears a projection on the rubber surface, tears and then rolls the tongue along the direction of sliding (Moore 1972). A critical value of shear stress can be defined for each rubber such that if the shear stress is higher than the critical shear stress, roll formation occurs and for shear stresses lower than the critical value, wear is mainly due to fatigue. Thus, the friction coefficient is one of the most important properties of rubber governing the type of wear. Hausberger has investigated the adhesive—and deformation- contribution to the friction and wear behavior of TPUs (Hausberger et al. 2018). He found that the ratio between the two frictional mechanisms is strongly influenced by the load, surface roughness, viscoelastic material behavior and ambient conditions.

In practice, a combination of three forms of wear occurs and it is difficult to separate the contribution of each mechanism to the overall wear (Moore 1972).

1.2. Stick-slip effect

Stick-slip is generally a dynamic cyclic process where two mating surfaces oscillate between a stick phase and a slip phase (Robert M. Gresham 2011). It is a widely observed phenomenon, ranging from the atomic to macroscopic scale, and from delicate instrumentation to daily life. Fig. 1 shows stick-slip behavior of elastomer slides on a smooth glass surface. Two different types of friction can contribute to stick-slip: static and kinetic friction. In the stick phase, the two surfaces are not in motion and are held in place by so-called static friction. In the slip phase, there is finite relative motion, so-called kinetic friction acts to retard this movement.

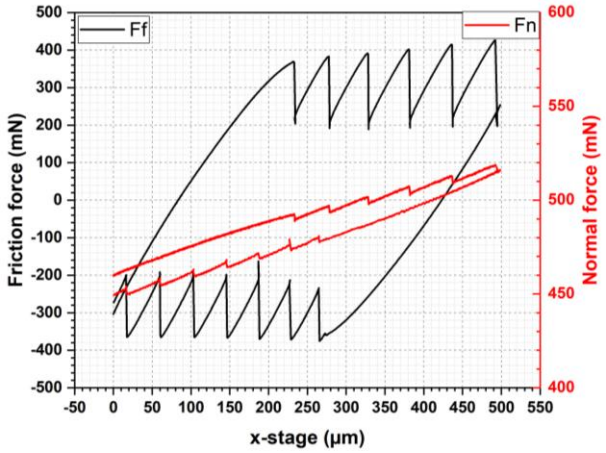

Fig. 1:Stick-slip behavior of elastomer against glass

For a given system, the stick-slip behavior can take place, when the static friction is greater than the kinetic friction. In general, the coefficient of friction increases as sliding velocity increases from very low speeds (10^{-6} mm/s), until reaching a maximum value around 1 to 100 mm/s. Sliding in this region is relatively uniform with no observable friction-induced oscillations. The friction force will fluctuate with the random variations that are present in all sliding tests due to variations in the mating surfaces. Above this critical velocity of peak friction, friction-induced vibration occurs. At velocities above the critical velocity, estimation of the friction values as a function of velocity is complicated due to the presence of friction-induced vibration. It appears that friction decreases with increasing velocity beyond the range of 1 to 100 mm/s (Rorrer 2000). The origin of stick-slip friction and characterization of its different friction mechanisms was conducted using liquid lubricants in a number of systems (Berman et al. 1996). Bengisu et al have investigated the dynamica of friction and the effect of surface roughness on stick-slip behavior by means of mathematical models (Bengisu and Akay 1999). They found that friction depends on both the interface properties of the surfaces and on the dynamic response of the system that embodies them.

The model relates macro-scale friction force to micro-scale forces developed at the true contact areas between surfaces. Expressing the contact forces in terms of contact areas and summing them statistically establishes this relationship. The significance of the deformation component of the friction force even if it is dominated by the adhesive component. Although the average friction force is essentially constant with respect to the mean sliding velocity of a friction platform, the deformation component of friction force shows a resonance-like behavior, reaching peak values at certain critical speeds. Stick–slip vibrations occur only in the presence of both deformation and adhesion components of frictional forces. An increase in surface roughness increases the strength of stick–slip motion, making it possible to develop even in the presence of large damping. On the other hand, changes in the magnitude of adhesive forces do not affect development of stick–slip as long as adhesive force magnitudes are above a certain threshold. This threshold roughly corresponds to the magnitude of the deformation forces. Gao (Gao et al. 1993) has studied the amplitude of the stick-slip motion of a multifiber slider as a function of the humidity, speed and applied load. In his study, the stick-slip amplitude is found to increase with increasing relative humidity and contact spot size, respectively, and to decrease with increasing substrate speed. Furthermore, the interfacial electrical resistance spikes at the beginnings of slip episodes and shows an unexpected hysteresis during stick-slip cycling. There is a critical speed beyond which no stick-slip motion occurs. This critical speed increases with increasing humidity and with increasing load, leading to increasing prevalence of stick-slip motion at higher loads and at higher humidities. Stick-slip motion is more persistent at higher loads and larger contact spot sizes, regardless of whether contact spots are elastic or plastic.

Stick-slip in seals can cause softening, swelling, binding, drag, wear, and even failure in a mechanism. Several factors that can affect the stick-slip behavior, e.g. material properties, surface roughness, fluid lubricity, contact pressure, temperature, and cycle speed. Liao et al has studied the stick-slip friction of reciprocating O-ring seals using acoustic emission techniques (Liao et al. 2012). It shows that both the AE RMS voltage and the friction coefficient vary with the stroke length are consistent. Corresponding to the different friction states in stick–slip friction, the AE characteristics represent close relationships with the tribological behaviors. Therefore, similar to the friction coefficient, the AE RMS voltage can reflect typical friction states in stick–slip friction. When the AE RMS voltage reached a maximum value, increased and decreased with the stroke length, the EPDM specimen was in transition from static to dynamic friction, partial slip, and slip

of low amplitude states, respectively. The AE RMS voltage increased with the normal load, which indicates that the normal load can intensify the AE activities of the specimen.

1.3. In situ tribometer

As we know, at microscopic level, solid surface consists of microscopic asperities. When two solid bodies come into contact, contacts occur through the asperities forming multiple asperity contact. This multiple asperity contact is essential in understanding sliding friction (Cohen and Tabor 1966; Greenwood and Tripp 1970). Ex situ methods can not reveal the physical phenomena occurring between the two contact surfaces at real time. Therefore, a new tool, in situ technique, is introduced in tribology. This technique is essential for fundamental studies of friction and wear because they are not intrinsic properties of a material; rather, they are functions of the tribological system (which includes the contacting surfaces that are in relative motion, the local environment, the background temperature, the surface roughness and preparation, the sliding speeds and loads, and a host of other contributors) (Sawyer and Wahl 2008). The factors in tribological systems were divided into three groups by Bowden and Tabor (Bowden and Tabor 1966). The first group includes the materials in contact and the contact geometry. The second group is about the operation conditions of tribological systems, including motion, loads, duration, etc. The third group consists of the environmental and surface conditions, including surface topography, surface chemistry, ambient temperature and humidity.

Fig. 2 shows the two common approaches of in situ tribological tests. At macroscale, two surfaces are in contact. Thus, the contact is a multi-asperity contact. The surface topography and wear generation that develop during testing can be observed between the two contact surfaces. With a proper data postprocessing it is possible to correlate the friction, wear generation with the surface topography. A serious limitation is that the analytical measurements are not carried out within the contact, so inferences need to be drawn between the observations outside the contact and the probable dynamics (chemical and mechanical) that exist within the contact (Sawyer and Wahl 2008). At nanoscale, it is possible to conduct the in situ measurement within only one contact. Different techniques were applied to nanoscale in situ tribology.

Chandrasekaran et al (Chandrasekaran and Batchelor 1997) has observed the abrasive wear of rubber using X-ray microscopy. In his study, he found that during sliding contact, the wearing contact area on rubber changes in shape and location. The changes in wearing contact area of rubber give rise to non-uniform wear of rubber. The frictional heating of the surface affects the behavior

of rubber by promoting thermal degradation under dry sliding conditions and consequently increases the wear rates upon continued sliding. Lubrication by mineral oil of sliding rubber specimens at elevated temperatures leads to accelerated wear at higher normal loads. Thermal degradation of rubber is promoted under high temperature lubrication leading to accelerated wear and chemical degradation of rubber. It is possible that the abrasive grains react with the rubber during sliding at high temperatures to form new compounds. Wang (Weiqiang and Shizhu 1994) has investigated the unlubricated wear process by means of a scanning electron microscope. He found that the adhesion force is in accordance with the theoretical values suggested using Bowden and Tabor's model. The wear surface can be divided into two areas, the real wear area and the transitional wear area. The wear mechanisms in the two areas are very different. The principal mechanism in the real wear area is adhesion. Particles mainly come from the real area. In the real wear area, the sizes of particles increase obviously along the sliding direction. When the real area is worn continuously, the original transitional area changes into a new real area. The untouched area changes into new transitional area when the number of particles increases.

To measure the friction and wear behavior of oil-lubricated metal surfaces, Korres et al (Korres and Dienwiebel 2010; Korres et al. 2012) have designed a tribometer. The surface topography with a three-dimensional (3D) holography microscope at a maximum frequency of 15 frames/s and higher resolution images are provided at defined time intervals by an atomic force microscope. The wear measurement is conducted online by means of radio nuclide technique. The quantitative measurement of the lateral and frictional forces is conducted with a custom-built 3D force sensor. Penkov et al (Penkov et al. 2017) have designed a micro tribotester for precise in situ wear measurements. It was found that transition of the wear mechanism from adhesive to abrasive wear took place when a significant amount of wear debris was formed as evidenced by the in situ observation of removal of the coating and exposure of the Si substrate. Schulze et al (Schulze et al. 2016) has investigated the real contact in a soft transparent interface by particle exclusion microscopy. They confirmed the technique by presenting a Hertz-like quasi-static indentation (loading time > 1.4 hrs) by a polyacrylamide probe into a stiff flat surface in a submerged environment. The real contact area and width were calculated from in situ images of the interface processed to reduce image noise and thresholded to define the perimeter of contact. Krick et al (Krick et al. 2012) have designed a optical in situ micro tribometer for analysis of real contact area for contact mechanics, adhesion, and sliding experiments. With this instrument it is possible to measure and observe contact size, contact geometry, near contact topography, tribofilm formation,

tribofilm motion, tribofilm thickness, wear debris formation, and wear debris morphology. Okamoto (Okamoto et al. 2007) has studied friction of elastomer on glass system using direct observation of its frictional interfaces. Viswanathan et al (Viswanathan et al. 2017) has studied the origin of stick-slip and surface wave propagation. It is shown that conventional post-mortem observation and inference can lead to erroneous conclusions with regard to formation of surface cracks and wear particles.

Varenberg (Murarash and Varenberg 2011) has used a special tribometer to operate inside an environmental scanning electron microscope enabling charge-free imaging of non-conductive and/or hydrated material. His study show direct link between precise data on the contact forces and images of the contact elements deformed by these forces indeed allows getting an insight into how contact surface patterns function when in contact. The technique of in situ transmission electron microscopy (TEM) has developed rapidly. The advent of improved cameras and continued developments in electron optics and stage designs have enabled scientists and engineers to enhance the capabilities of previous TEM analyses (Ferreira et al. 2008). Liao and Marks (Liao and Marks 2017) have studied a single asperity wear at the nanometer scale with in situ TEM technique.

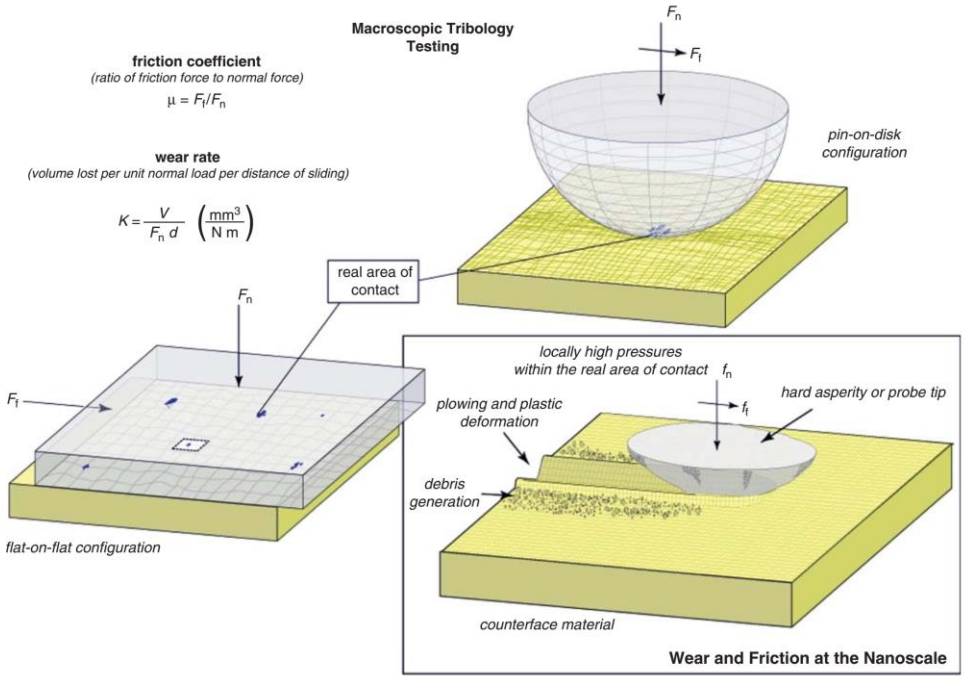

Fig. 2: In situ tribological tests at macro- and microscale (Sawyer and Wahl 2008).

2. Experimental details

All tests were conducted on a in situ microtribometer at the Material Tribology Laboratory at the University of Illinois at Urbana-Champaign.

2.1. In situ microtribomter

The in situ microtribometer consists of two parts, the tribometer (Fig. 3) and the optical observation system. With this setup it is possible to perform various tests with observation of the contact area, e.g. indentation, creep, relaxation, friction tests. Before a test, a specimen is mounted directly to the head of a flexure. There are two capacitance probes at the head of the flexure, one is normal to the contact and the other one is in the sliding direction. Depending on the stiffness of the flexure, two capacitive sensors are responsible to measure the deflection of the flexure in vertical and horizonal directions, which deliver the friction and normal forces during the tests (Fig. 4). The flexure is mounted on a vertical piezoelectric stage, which provides control over the displacement of the probe. Furthermore, a micrometer screw stages enable a precise position of the sample and the probe in range. As counter part, commercial microscope slides were employed. The micro tribometer was controlled through LabView.

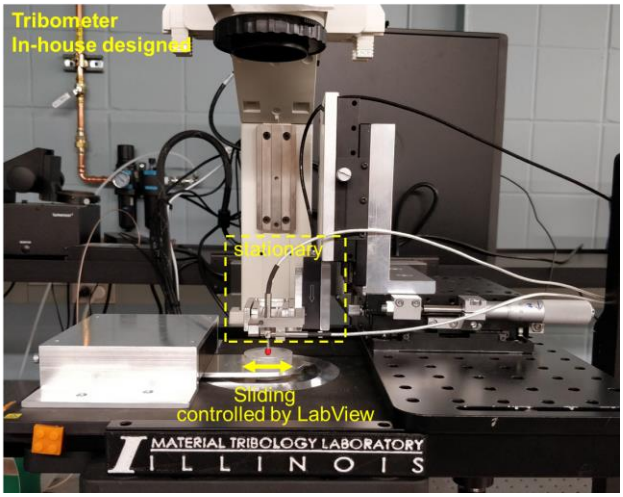

Fig. 3: Optical in situ microtribometer

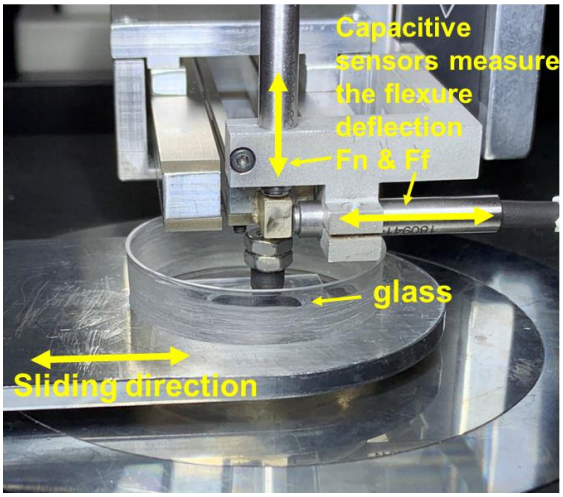

Fig. 4: Capacitive sensors and flexure.

Beneath the sample and counter part is a microscope objective facing upward toward the sample. The counter part was mounted on a piezoelectric stage that generates sliding movement. The microscopic optical observation system is mounted beneath the counter part. A microscope (Inverted research microscope Eclipse Ti, Nikon, Japan) with an objective (4x) was employed to observe the contact area through a transparent counter part. The contact area was illuminated

through a LED ring illuminator. (64 LEDs). Images are acquired with NIS-Elements (Ver. 4.0, Nikon). The selected frame rate is about 20 frames per seconds.

2.2. Test materials & sample

Fluoroelastomer (FKM) and hydrogenated nitrile butadiene rubber (HNBR), two classical sealing material, were as sample investigated in this study. The sample was manufactured through turning process. The whole sample has a cylindrical form with a length of 5.17 mm. One side of the sample, which is the contact area, is a hemisphere with a diameter of 4.86 mm. FKM has a shore-A hardness of 84, while HNBR is a bit harder and its hardness of HNBR is 86. Prior to the experiment, the topography of the sample was characterized with a three-dimensional focus variation microscope (InfiniteFocus, Alicona, Graz, Austria) and an optical light microscope (Stereo Microscope SZX 12, Olympus, Tokyo, Japan). As shown in Fig. 5, after manufacture the turning marks can still be observed on the sample surface. Fig. 6 shows the roughness and waviness of FKM sample topography. The surface has a roughness (Ra) of 1.286 µm and a Rsm of 104.2 µm. Its waviness (Wa) is 50.23 µm.

Fig. 5: 2D (left) and 3D (middle) graphics of FKM hemispherical sample; 2D graphic of HNBR sample (right)

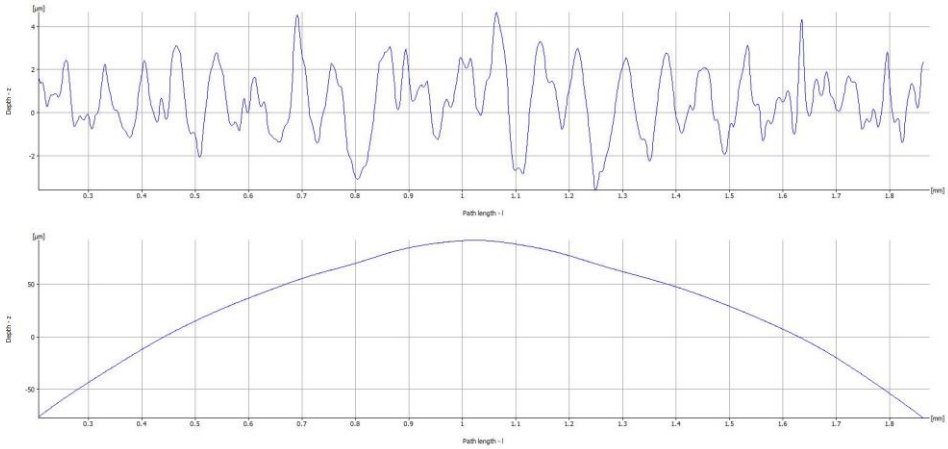

Fig. 6:Roughness (up) and waviness (down) of the topography of FKM

2.3. Test parameter

For the stick-slip tests, the sample is pressed on the counter part with a normal load of 500 mN. The trace length is 500 µm. Each cycle consists of two traces, namely trace and retrace. In order to investigate the influence of sliding speeds on the stick-slip behavior, four different speeds were selected to conduct the tests. It ranges from 100 µm/s, over 20 µm/s, 5 µm/s to 1 µm/s. The number of cycles depends mainly on the time, when the stick-slip behavior completely disappeared during the test.

Table 1. Test parameter of stick-slip tests

FKM	Normal load [mN]	Length per trace [µm]	Speed [µm/s]	Number of cycles [-]
Test_1	500	500	100	200
Test_2	500	500	20	20
Test_3	500	500	5	30
Test_4	500	500	1	7

The creep test was conducted with the same setup. The normal load was 800mN. The sample was loaded with a load rate of 50 mN/s. The creep test aims to check the deformation of the contact area with time.

2.4. Video processing

The postprocessing of video was performed with two methods. The first method is an open source software – ImageJ, which was developed at the National Institutes of Health (NIH) and the Laboratory for Optical and Computational Instrumentation (LOCI, University of Wisconsin). At first, the single frame is cut, so that only the contact relevant area stays in the frame. It is a useful way to reduce noises. Secondly, the original RGB color frame, which consists of three additive primary colors, red, green, and blue, split to a single color, normally red. Then, the single color frame is thresholded, it should be manually adjusted to the real contact area. Additionally, there is a powerful tool in ImageJ, called analyze particles (Fig. 7). Using this tool, all the contact asperities can be analyzed automatically, including number of the asperities, size, total number, total area and percentage of contact area to the whole area. The advantage of ImageJ is its open source and easy usage. However, its limitation is also quite obvious. It can only process a single frame every time. For video processing it is very time consuming.

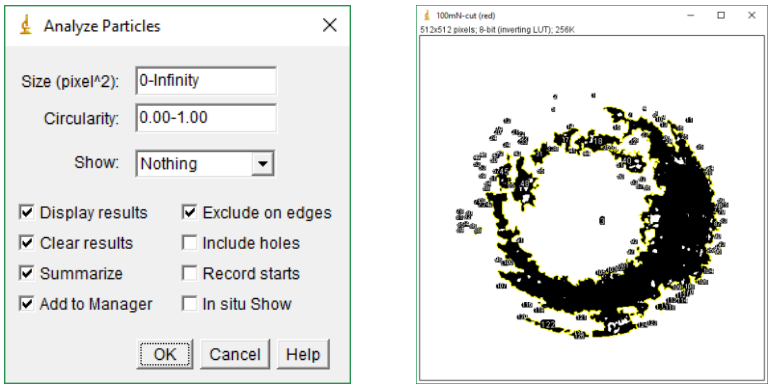

Fig. 7: Function of analyze particles in ImageJ

To process a whole video, the second method was employed. MATLAB programs were used to obtain the contact area from each frame in a video automatically. Similar to the first method, each frame is cut to keep the relevant contact region in the frame. The cropped frames are exported with the same frame rate as the original video. The next step is to find out the first frame in the loading phase, in which the contact occurs. A number of frames at the beginning of the test are exported as single frames. Then each of these frames subtracts the first frame, so that it is obvious to find out the first contact frame and where the first contact is (Fig. 8). The frames prior to the contact is irrelevant and will not be considered in the following processes. The following steps are different for creep tests and sliding stick-slip tests.

For creep test, only vertical movement and no horizontal movement undertakes during the test. Therefore, the contact area can be identified with the previous method. All of the frames subtract the first contact frame and export all processed frames with the original frame rate. Each frame are thresholded using Otsu's method (Otsu 1979). This method enables an automatic reduction of gray level image to binary image. The method is based on the zero-th and the first order cumulative moments of the gray level histogram. It involves iterating through all the possible threshold values and calculating a measure of spread for the pixel levels each side of the threshold, i.e. the pixels that either fall in foreground or background. The aim is to find the threshold value where the sum of foreground and background spreads is at its minimum. After thresholding, the bright pixels are counted, which represent the contact area. Conversely, the dark pixels stand for the non-contact area.

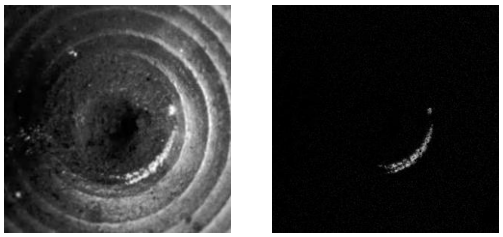

Fig. 8:The original frame (left) and processed frame (right)

For sliding stick-slip tests, the subtract method does not work, because the sample deforms with the horizonal movement of the counter part to some extent. Hence, each frame is directly thresholded after crop.

3. Results & discussion

The HNBR indentation was evaluated with ImageJ. The creep tests and sliding stick-slip tests were postprocessed with MATLAB programs. At first, the results of indentation test with HNBR are discussed. It shows the change of the contact area along with increasing normal load. Here FKM is chosen as an example to show the creep tests and sliding stick-slip tests. The video was processed with MATLAB program, so that the change of contact area with test time was obtained.

3.1. Indentation and Creep test

3.1.1 Indentation test with HNBR

For the indentation test with HNBR, the sample was loaded stepwise with an interval of 100 mN. The normal load ranges from 100 mN to 800 mN. After each load, an image of the contact area was taken. As can be seen in Table 2, the contact area increases with in creasing normal load. After postprocessing, it is clear to identify the contact area. The contact area increases according to the turning marks. When the normal load increases from 400 mN to 500 mN, the edge, which was produced by turning process, comes into contact prior to the other part. Under 100 mN normal load, there was still space around the contact area, which is not in contact. With increasing normal load, this space comes also into contact.

Table 2: Contact areas prior to threshold and after threshold of the indentation test with HNBR

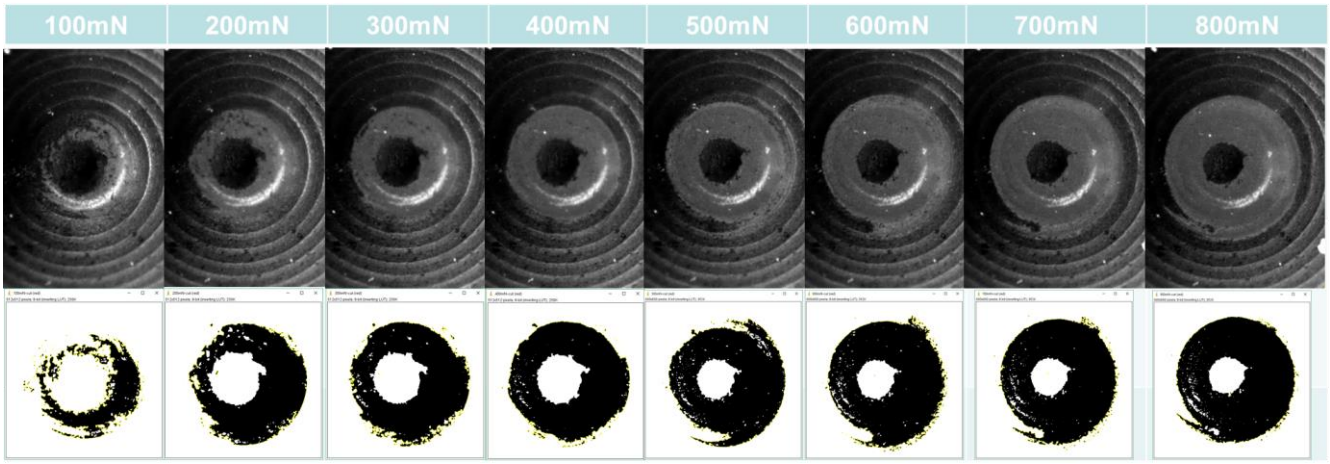

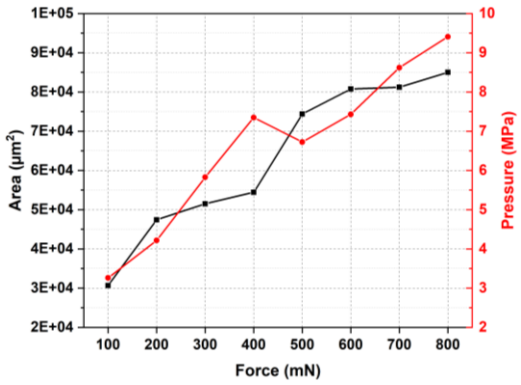

Fig. 9:Change f contact area and contact pressure with increasing normal load

Fig. 9 shows the change of contact area and contact pressure with increasing normal load. When the normal load increases from 400 mN to 500 mN, the contact area increases from 5.5×10^4 to 7.5×10^4. This can be attributed to the change of contact area. As can be seen in Table 2, the outer ring comes into contact, which reduced the average contact pressure from 7.4 MPa to 6.7 MPa. After 500 mN the average contact pressure increases with increasing normal force. The average contact pressure reached 9.4 MPa with a normal load of 800 mN.

3.1.2 Creep test with FKM

The creep tests were designed to check the alteration of contact area within a period of time. This viscoelastic deformation process can also be identified in the sliding tests. It is one of the contributions of contact area increase. The creep tests were conducted with a normal load of 800 mN. The FKM sample was loaded with a load rate of 50 mN/s to 800 mN. After reached the maximum load, the normal force kept constant for over 18 minutes. The contact area was observed with a microscope and camera from the beginning of the loading phase. As shown in Fig. 10, after

loading phase, the contact area increased slowly with time and reached 21580 µm^2 after 18 minutes. To get a continuous information of the contact area change, the video of contact areas was postprocessed with MATLAB Programs.

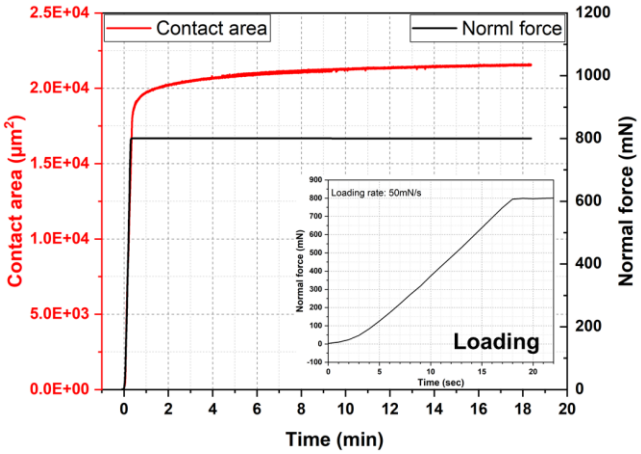

Fig. 10:Creep test of FKM with a normal load of 800 mN

3.2. Stick-slip behavior

Stick-slip behaviors were identified in all four tests. However, the sliding speed is of great importance of the stick-slip behavior. Within each test, the stick-slip behavior changed with cycles. In addition, the contact area changes with stick-slip behaviors.

3.2.1. General description

Due to the low elasticity of FKM and also the hemisphere geometry of specimens, slight movement of contact area can be identified when the counter part moves. As can be seen in Fig. 11, as the counter part (glass) moves from one side of the trace (x = -250 µm) to the other side of the trace (x = +250 µm), the frictional force reached 220 N during the stick stage until the first slip took place. At that moment, the counter part has already moved around 250 µm. In other words, the specimen at the contact area has moved with the counter part together for about 250 µm before it reached its deformation limit. After the counter part reached the other side of the trace, it turned back, and the stick-slip process started again for retrace.

Within each test, the stick-slip behavior changes with cycles. In this study, the alteration of stick-slip frequency, amplitude of stick and slip, change of friction force and coefficient of friction (COF) were investigated. With increasing cycles, the interface changes, hence, the stick-slip behavior alters accordingly. Depends on the test parameters, the stick-slip behavior declines gradually until it disappears totally. For Test_1 and Test_2, the stick-slip behavior can not be observed after around

20 cycles, while it can still be identified after 30 cycles for Test_3. For the test with the lowest sliding speed, the stick-slip behavior disappears after merely four cycles.

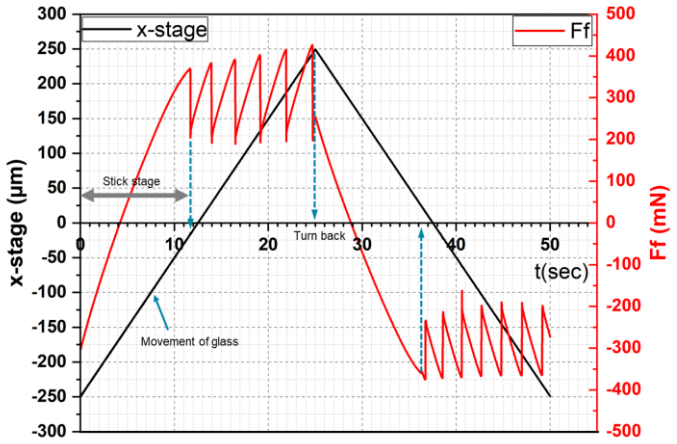

Fig. 11:Movement of specimen and glass during sliding tests from Test_2.

3.2.2. Comparison of different tests

The influence of sliding speed can be identified with friction force (Ff) and coefficient of friction (COF), in particular in the first cycle. As can be seen in Table 3, considerable difference can be observed, especially at low speeds. Only focusing on the trace part, for the tests with a decreasing sliding speeds, namely from 100 µm/s to 5 µm/s, 8, 6 and 4 slips took place during the first trace in Test_1, Test_2, and Test_3, respectively. Therefore, the number of slips reduces with decreasing sliding speeds. However, Test_4 with a sliding speed of 1 µm/s experienced 15 slips in the first trace. This can be inferred that the adhesive bonds in the interface get separated slowly, if the elastomeric material has enough time to recover (Sills et al. 2007). During the stick-slip movement, the penetration depth changes, therefore, the normal force changes slightly. This phenomenon is in good agreement with the results from (Fukahori et al. 2010). In term of reduction of friction force during the slip stage, the largest reduction can be identified in Test_3, which has an average reduction of 245 N in the first trace. It is also obvious that the smallest reduction of friction force undertook in Test_4, with an average value of around 50 N, which is almost only one fifth of it in Test_3. For Test_1 and Test_2, it is 130 N and 210 N, respectively. As shown in Table 3, except for Test_4, the reduction of friction force increased slightly during the first trace in all other tests. This phenomenon can be observed in the retrace movement as well.

Table 3:Comparison of the first cycle in four tests

Test_1 (100 µm/s)	Test_2 (20 µm/s)

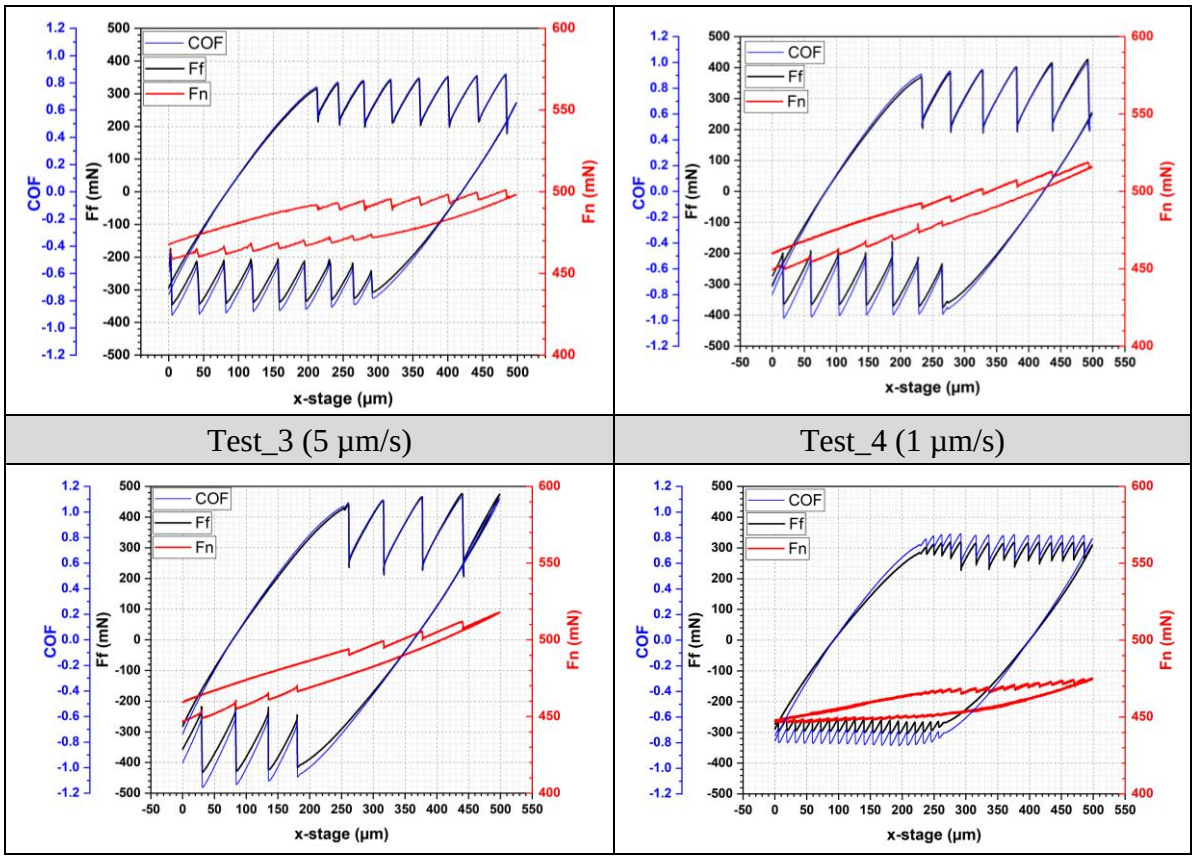

Test_3 (5 μm/s) | Test_4 (1 μm/s)

Fig. 12 shows the relations of stick-slip frequency and sliding frequency. The sliding frequency is calculated from the sliding speed and the length of trace. The different stick-slip frequencies values at the same sliding frequency indicate that the values come from one test, but different cycles. It is obvious that high sliding speeds enable a more frequent stick-slip behaviors. The data fits well with Eq. 1. To fit the curve, the average stick-slip frequency at each sliding frequency was used. Only Test_2 with a sliding speed of 20 μm/s is slightly beyond the exponential growth curve.

$$y = 0.30363 * e^{\left(\frac{x}{0.08682}\right)} - 0.2372 \qquad \text{Eq. 1}$$

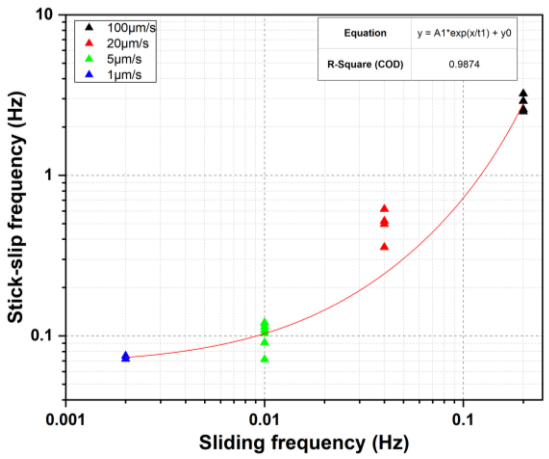

Fig. 12: Relation of stick-slip frequency and sliding frequency

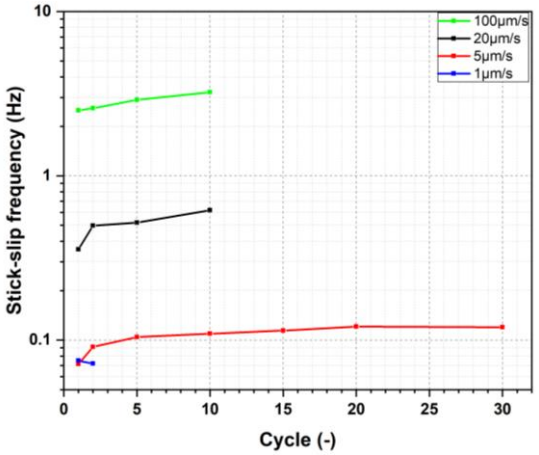

Fig. 13: Relation of stick-slip frequency with cycles in each test

The relation of stick-slip frequency and cycle number is shown in Fig. 13. Except for Test_4 with a sliding speed of 1 μm/s, all the other three tests experienced an increase in stick-slip frequency with increasing cycles. Especially for Test_2 and Test_3, an obvious increase in stick-slip frequency can be identified after the first cycle. After the first cycle, the frequency kept almost at the same level until the stick-slip behavior disappear. However, for Test_4, the stick-slip frequency decreased slightly. The stick-slip behavior can only be observed in the first cycle of Test_4. Moreover, in the third cycle, as shown in Fig. 14, merely unregular stick-slip behavior can be identified in the trace movement.

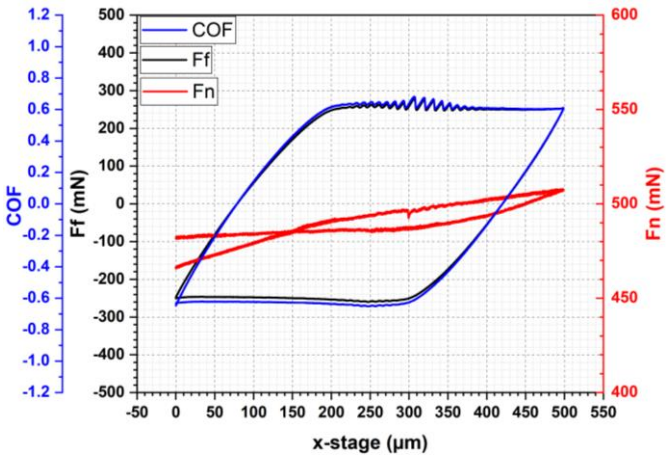

Fig. 14: The third cycle of Test_4.

3.3. Visualization of the real contact area

The contact area was measured with an optical system, including microscope and camera. The calculation was conducted with MATLAB programs. As can be seen in Fig. 15, the contact area changes with the stick-slip behavior. It reached its maximum value at the point, when the glass

turned back. This can be attributed to two reasons. The one is that at the turning point, the specimen experiences the maximum deformation due to the shear stress. Therefore, the contact area became larger. When the glass started to move in the other direction, the deformation became smaller again, hence, the contact area reduced accordingly. Similar to the trace movement, the contact area changes with the stick-slip behavior in the retrace movement as well. However, the amplitude of change in contact area is milder. This phenomenon is resulted from the smaller average reduction of friction force in retrace movement comparing to trace movement.

Compared with the first trace, the contact area in the 10th cycle is generally larger (Fig. 15). As mentioned previously, this phenomenon can be traced back to two reasons, namely the viscoelasticity of material and the interface change along the sliding test. It is also obvious that the change of contact area during the stick-slip behavior is considerably smaller in 10th cycle than in the first cycle. This can be attributed to the milder stick-slip behavior, which means chiefly a smaller alteration of friction force.

Accordingly, when the stick-slip behavior can not be identified in the sliding test, no obviously regular alteration of contact area can be identified along sling test. After 20 cycles, the specimen slid smoothly over the counter part and no stick-slip behavior exists in the interface. As can be observed in Fig. 15 (right), the periodical increase and decrease of contact area between trace and retrace can still be identified. However, a regular change of contact area within the trace or retrace can not be identified any more.

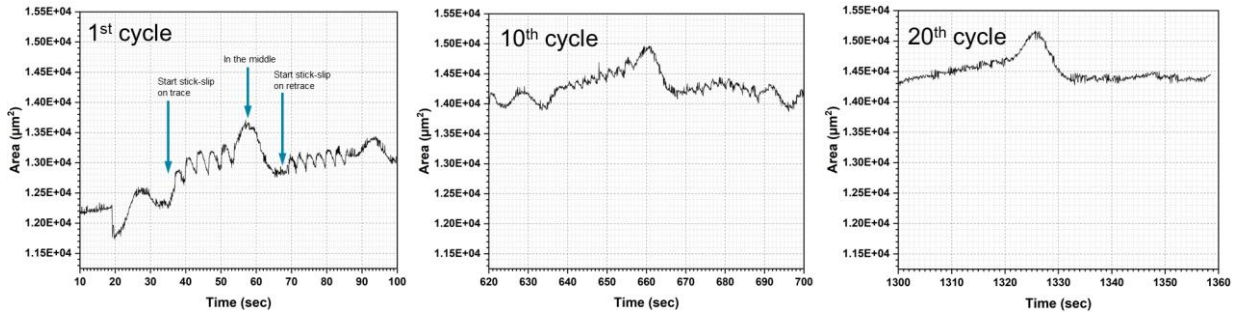

Fig. 15:Change of contact area with time in the first (left), 10th (middle), and 20th (right) trace from Test_2.

3.3.1. Stick region in contact area

For plastic materials, the entire real contact area is composed of two regions, stick region (2c) and slip region (2a) (Eguchi et al. 2009). The stick region moves together with the counter part and undertakes an elastic or even slightly plastic deformation until the tangential force reaches the maximum static friction force. In the slip region, a local slip takes place along with the movement

of counter part. The stick and slip regions change with cycles due to the alteration of interface. In addition, within each trace or retrace, the two regions do not keep at a constant value. This phenomenon can be attributed to the shear deformation, which is mainly dependent on the relative position of the specimen on trace. The shear stress is at its minimum level, when the specimen is at one of the sides of the trace and shortly after the counter part changes its moving direction. At this moment, the shear stress is balanced. The shear stress reaches its maximum value before the glass changes its moving direction. The shear stress becomes larger, when the counter part moves from one side to the side. With increasing shear stress, as a consequence, the area of stick region changes accordingly.

To calculate the stick region, the counter part is applied as the frame of reference. The stick region adheres to the counter part and moves together. Hence, the stick region does not experience any relative movement. Therefore, from a view of counter part, the immobile area is the stick region. As can be seen in Fig. 16, the whole contact region is marked with yellow lines and the overlapped region is marked with red line. The overlapped region between the first and fortieth frame is the stick region. Before being subtracted by the fortieth frame, the first frame was adjusted according to the movement of the counter part during the time.

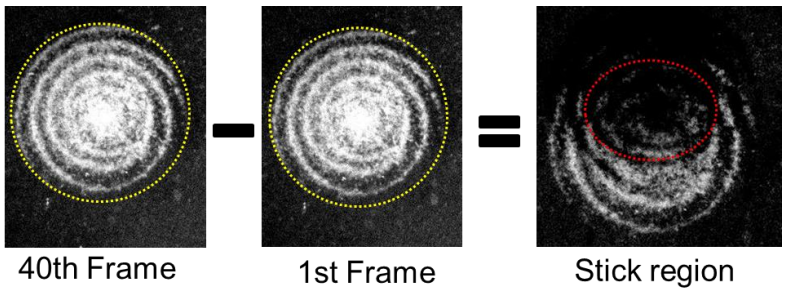

Fig. 16:Process to calculate the stick region.

In this study, we observed stick and slip regions during the sliding tests and also their change was investigated. In addition, comparison among the four tests was conducted and the influence of sliding speeds on the change of stick and slip region was concluded. In Fig. 17, the stick region (c) and the whole contact region (a) of all four tests were shown. The Test_4 has a larger whole contact region, accordingly the stick region is also larger than that in the other three tests. The creep effect must be taken into consideration. With 1 µm/s sliding speed, its cycle time is much longer than other tests. Therefore, the viscoelasticity of material shows an impact on the contact area. In addition, generally for elastomer, the material shows a higher storage modulus, when the test

frequency becomes higher. For Test_4, its test frequency is 0.002 Hz, which is much lower than other tests. Meanwhile, its cycle time is much longer than other tests. Hence, the contact area is slightly larger. For stick region, all other three tests do not have significant difference at the first cycle. However, after five cycles, the stick region started to grow at different extents. As to the whole contact area, only slight difference can be identified among the three tests.

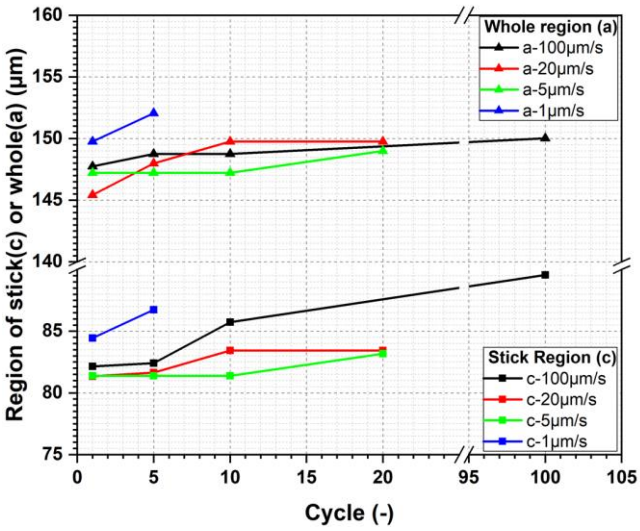

Fig. 17: Change of stick and slip regions with cycles.

3.3.2. Correlation of friction and real contact area

With the help of the observation of the contact area during the sliding tests, it is possible to correlate the measured friction force with the contact area, in particular for the stick-slip behaviors. The in situ technique enables a direct combination of material deformation in normal, tangential directions and the measured normal and tangential force in real time. It has a direct and significant contribution to the friction behavior.

Fig. 18 shows the alteration of contact area along with stick-slip behavior. It can be observed that the contact area decreased during the stick phase and increased abruptly with the slip movement of the specimen. It can be assumed that the whole contact area deformed largely as a consequence of the shear stress. The outer region of the contact area, in particular the slip region, may experience a transition from the contact state to non-contact state. In prior to the first slip, a precursor can be identified in Fig. 18. This phenomenon can also be found in (Rubinstein et al. 2009). The friction force increased in a nearly linear way until reaching a peak force. At the peak point, the friction force dropped abruptly from over 400 N to around 200 N. At the same time, the friction transforms from static friction to dynamic friction. This transformation took place in around 30 milliseconds.

Taking a close look at the loading curve, before reaching the peak force, a small drop (around 1 %) of friction force during the load phase can be identified. Bennewitz et al (Bennewitz et al. 2008) conducted a set of experiments where an engineered PDMS tip array was sheared over polished glass surface. It was found that sliding is preceded by crack-like precursors that cause compressive strain to form along the interface. When shear load is applied to the edge of the sliding block it is natural to assume the existence of some mechanism that transfers the stresses across the frictionally bound interface during loading. They found that the physical process of sliding movement can be divided into three steps. In the first stage, the elastomer sample deforms under the shear stress without changing the strain in the contact. In the next stage, a compressive strain is built up. The compression runs usually in the form of step-like increases, reminiscent of crack-like precursors to sliding (Bennewitz et al. 2008). In the third step, the contact begins to slip in a stick slip movement that manifests as a periodic change in the strain. It is believed that the stick-slip comes from the random roughness of the glass surface and that its regularity results from a folding with the regular structure of the sample tip.

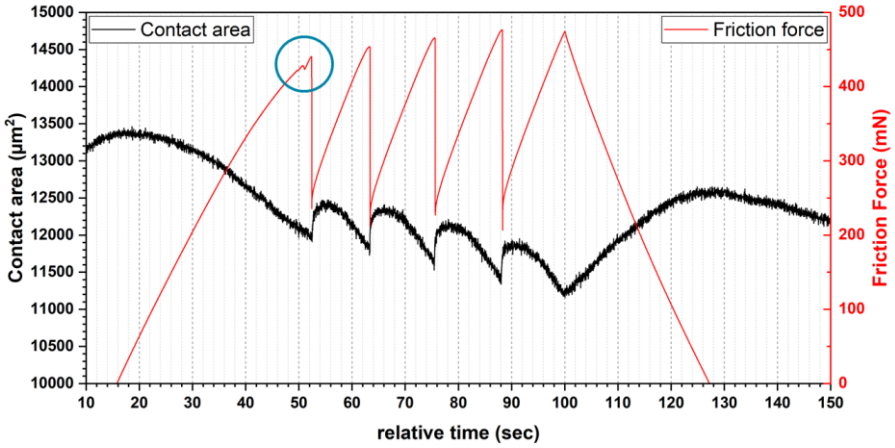

Fig. 18:Change of the contact area within the stick-slip behavior of the first trace in Test_3.

4. Conclusion

The contact area and the stick-slip behavior of a hemispheric elastomer sliding on a polished glass by using an in situ micro tribometer were investigated. Except for the sliding tests, creep tests and indentation tests were conducted and the real contact area during the tests were analyzed. To postprocess the videos, two methods were developed and applied. The effects of sliding speed on the stick-slip behavior and the alteration of real contact area were studied by comparison of different tests, conducted with a range of sliding speed from 100 μm/s to 1 μm/s. In addition, the stick region and slip region in the real contact area were observed and studied. Moreover, their

relations with sliding speeds and cycle numbers were clarified and then possible factors affecting the change were investigated. Based on the presented results and discussion, the following conclusions can be drawn:

1) In the indentation tests, due to the turning marks on the specimen surface, the real contact surface does not increase with increasing normal load continuously. Hence; the average contact pressure variates.
2) In the sliding tests, stick-slip effects were observed in all tests, conducted with a range of sliding speed from 100 μm/s to 1 μm/s.
3) When the sliding speeds are between 100 μm/s to 5 μm/s, the number of slips reduces with decreasing sliding speeds. However, in case of a sliding speed of 1 μm/s, slip took place more frequently than all other tests.
4) Generally, the frequency of stick-slip effects decreases with increasing cycle numbers. The stick-slip behavior can be observed in a high cycle number, if the sliding speed is high.
5) For stick region, except for the 1 μm/s test, all other three tests do not have significant difference in the first cycle. After five cycles, the stick region started to grow at different extents. As to the whole contact area, only slight difference can be identified among the three tests.
6) The contact area decreased during the stick phase and increased abruptly with the slip movement of the specimen. The transformation from static friction to dynamic friction took place in around 30 milliseconds.
7) In the stick phase, before reaching the peak force, a small drop (around 1 %) of friction force during the load phase was found.

Acknowledgment

The author would like to express appreciation to A. Hausberger, J. Kim, S. Bonyadi, C. Johnson and L. Wei for their technical support. The present research was partially finally supported by Marshall-Plan Foundation and it was carried out at the Materials Tribology Laboratory of the University of Illinois at Urbana-Champaign in the USA and Polymer Competence Center Leoben GmbH in Austria, within the framework of the Competence Center Program COMET by the Federal Ministry of Transport, Innovation and Technology and the Federal Ministry of Economics, Family and Youth, with the participation of the Chair of Mechanical Engineering and the Chair of Materials Science and Testing of Polymers, Montanuniversität Leoben, SKF Sealing Solutions

Austria GmbH and partially funded by federal and state governments of Styria, Lower Austria and Upper Austria.

Publication bibliography

Barquins, M.; Courtel, R. (1975): Rubber friction and the rheology of viscoelastic contact. In *Wear* 32 (2), pp. 133–150. DOI: 10.1016/0043-1648(75)90263-X.

Belyi, V. A.; Sviridyonok, A. I.; Smurugov, V. A.; Nevzorov, V. V. (1977): Adhesive Wear of Polymers. In *J. Lub. Tech.* 99 (4), p. 396. DOI: 10.1115/1.3453232.

Bengisu, M. T.; Akay, Adnan (1999): Stick–slip oscillations: Dynamics of friction and surface roughness. In *The Journal of the Acoustical Society of America* 105 (1), pp. 194–205. DOI: 10.1121/1.424580.

Bennewitz, Roland; David, Jonathan; Lannoy, Charles-François de; Drevniok, Benedict; Hubbard-Davis, Paris; Miura, Takashi; Trichtchenko, Olga (2008): Dynamic strain measurements in a sliding microstructured contact. In *Journal of physics. Condensed matter : an Institute of Physics journal* 20 (1), p. 15004. DOI: 10.1088/0953-8984/20/01/015004.

Berman, Alan D.; Ducker, William A.; Israelachvili, Jacob N. (1996): Origin and Characterization of Different Stick−Slip Friction Mechanisms †. In *Langmuir* 12 (19), pp. 4559–4563. DOI: 10.1021/la950896z.

Bowden, F. P.; Tabor, D. (1966): Friction, lubrication and wear: a survey of work during the last decade. In *Br. J. Appl. Phys.* 17 (12), pp. 1521–1544. DOI: 10.1088/0508-3443/17/12/301.

Chandrasekaran, Margam; Batchelor, Andrew William (1997): In situ observation of sliding wear tests of butyl rubber in the presence of lubricants in an X-ray microfocus instrument. In *Wear* 211 (1), pp. 35–43. DOI: 10.1016/S0043-1648(97)00037-9.

Cohen, S. C.; Tabor, D. (1966): The Friction and Lubrication of Polymers. In *Proceedings of the Royal Society A: Mathematical, Physical and Engineering Sciences* 291 (1425), pp. 186–207. DOI: 10.1098/rspa.1966.0088.

Eguchi, Masao; Shibamiya, Takashi; Yamamoto, Takashi (2009): Measurement of real contact area and analysis of stick/slip region. In *Tribology International* 42 (11-12), pp. 1781–1791. DOI: 10.1016/j.triboint.2009.04.046.

Ferreira, P. J.; Mitsuishi, K.; Stach, E. A. (2008): In Situ Transmission Electron Microscopy. In *MRS Bull.* 33 (02), pp. 83–90. DOI: 10.1557/mrs2008.20.

Flitney, Robert K. (2014): Seals and sealing handbook. Sixth edition. Amsterdam, Boston, Heidelberg: BH Butterworth-Heinemann an imprint of Elsevier (Butterworth-Heinemann/IChemE series).

Fukahori, Y.; Gabriel, P.; Busfield, J.J.C. (2010): How does rubber truly slide between Schallamach waves and stick–slip motion? In *Wear* 269 (11-12), pp. 854–866. DOI: 10.1016/j.wear.2010.08.016.

Gao, Chao; Kuhlmann-Wilsdorf, Doris; Makel, David D. (1993): Fundamentals of stick-slip. In *Wear* 162-164, pp. 1139–1149. DOI: 10.1016/0043-1648(93)90133-7.

Greenwood, J. A.; Tripp, J. H. (1970): The Contact of Two Nominally Flat Rough Surfaces. In *Proceedings of the Institution of Mechanical Engineers* 185 (1), pp. 625–633. DOI: 10.1243/PIME_PROC_1970_185_069_02.

Grosch, K. A. (1963): The Relation between the Friction and Visco-Elastic Properties of Rubber. In *Proceedings of the Royal Society A: Mathematical, Physical and Engineering Sciences* 274 (1356), pp. 21–39. DOI: 10.1098/rspa.1963.0112.

Hausberger, A.; Major, Z.; Theiler, G.; Gradt, T. (2018): Observation of the adhesive- and deformation- contribution to the friction and wear behaviour of thermoplastic polyurethanes. In *Wear* 412-413, pp. 14–22. DOI: 10.1016/j.wear.2018.07.006.

Heinrich, Gert (1997): Hysteresis Friction of Sliding Rubbers on Rough and Fractal Surfaces. In *Rubber Chemistry and Technology* 70 (1), pp. 1–14. DOI: 10.5254/1.3538415.

Johnson, K. L. (1997): Adhesion and friction between a smooth elastic spherical asperity and a plane surface. In *Proceedings of the Royal Society A: Mathematical, Physical and Engineering Sciences* 453 (1956), pp. 163–179. DOI: 10.1098/rspa.1997.0010.

Johnson, K. L.; Kendall, K.; Roberts, A. D. (1971): Surface Energy and the Contact of Elastic Solids. In *Proceedings of the Royal Society A: Mathematical, Physical and Engineering Sciences* 324 (1558), pp. 301–313. DOI: 10.1098/rspa.1971.0141.

Korres, Spyridon; Dienwiebel, Martin (2010): Design and construction of a novel tribometer with online topography and wear measurement. In *Review of Scientific Instruments* 81 (6), p. 63904. DOI: 10.1063/1.3449334.

Korres, Spyridon; Feser, Tim; Dienwiebel, Martin (2012): In situ observation of wear particle formation on lubricated sliding surfaces. In *Acta Materialia* 60 (1), pp. 420–429. DOI: 10.1016/j.actamat.2011.09.046.

Krick, Brandon A.; Vail, Jennifer R.; Persson, Bo N. J.; Sawyer, W. Gregory (2012): Optical In Situ Micro Tribometer for Analysis of Real Contact Area for Contact Mechanics, Adhesion, and Sliding Experiments. In *Tribol Lett* 45 (1), pp. 185–194. DOI: 10.1007/s11249-011-9870-y.

Liao, Chuanjun; Suo, Shuangfu; Wang, Yuming; Huang, Weifeng; Liu, Ying (2012): Study on Stick–Slip Friction of Reciprocating O-Ring Seals Using Acoustic Emission Techniques. In *Tribology Transactions* 55 (1), pp. 43–51. DOI: 10.1080/10402004.2011.626145.

Liao, Y.; Marks, L. (2017): In situ single asperity wear at the nanometre scale. In *International Materials Reviews* 62 (2), pp. 99–115. DOI: 10.1080/09506608.2016.1213942.

Maeda, Nobuo; Chen, Nianhuan; Tirrell, Matthew; Israelachvili, Jacob N. (2002): Adhesion and friction mechanisms of polymer-on-polymer surfaces. In *Science (New York, N.Y.)* 297 (5580), pp. 379–382. DOI: 10.1126/science.1072378.

Moore, D. F.; Geyer, W. (1972): A review of adhesion theories for elastomers. In *Wear* 22 (2), pp. 113–141. DOI: 10.1016/0043-1648(72)90271-2.

Moore, D. F.; Geyer, W. (1974): A review of hysteresis theories for elastomers. In *Wear* 30 (1), pp. 1–34. DOI: 10.1016/0043-1648(74)90055-6.

Moore, Desmond F. (1972): The friction and lubrication of elastomers. [1st ed.]. Oxford, New York: Pergamon Press (International series of monographs on materials science and technology, v. 9).

Murarash, B.; Varenberg, M. (2011): Tribometer for In Situ Scanning Electron Microscopy of Microstructured Contacts. In *Tribol Lett* 41 (2), pp. 319–323. DOI: 10.1007/s11249-010-9717-y.

Myshkin, N. K.; Petrokovets, M. I.; Kovalev, A. V. (2005): Tribology of polymers. Adhesion, friction, wear, and mass-transfer. In *Tribology International* 38 (11-12), pp. 910–921. DOI: 10.1016/j.triboint.2005.07.016.

Nikas, G. K. (2016): Eighty years of research on hydraulic reciprocating seals. Review of tribological studies and related topics since the 1930s. In *Proceedings of the Institution of Mechanical Engineers, Part J: Journal of Engineering Tribology* 224 (1), pp. 1–23. DOI: 10.1243/13506501JET607.

Okamoto, Yoshihiro; Nishio, Kazuyuki; Sugiura, Jun-ichi; Hirano, Motohisa; Nitta, Takahiro (2007): Friction of elastomer-on-glass system and direct observation of its frictional interface. In *J. Phys.: Conf. Ser.* 89, p. 12011. DOI: 10.1088/1742-6596/89/1/012011.

Otsu, Nobuyuki (1979): A Threshold Selection Method from Gray-Level Histograms. In *IEEE Trans. Syst., Man, Cybern.* 9 (1), pp. 62–66. DOI: 10.1109/TSMC.1979.4310076.

Penkov, Oleksiy; Khadem, Mahdi; Nieto, Andy; Kim, Tae-Hyeong; Kim, Dae-Eun (2017): Design and Construction of a Micro-Tribotester for Precise In-Situ Wear Measurements. In *Micromachines* 8 (12), p. 103. DOI: 10.3390/mi8040103.

Redesigning the space shuttles solid rocket motor seals (1996). In *Sealing Technology* 1996 (26), pp. 10–12.

Robert M. Gresham (2011): Slip-stick: What's it all about? In *Tribology & Lubrication Technology* 06, pp. 32–33.

Rorrer, Ronald A. L. (2000): A Historical Perspective and Review of Elastomeric Stick—Slip. In *Rubber Chemistry and Technology* 73 (3), pp. 486–503. DOI: 10.5254/1.3547601.

Rubinstein, S. M.; Cohen, G.; Fineberg, J. (2009): Visualizing stick–slip: experimental observations of processes governing the nucleation of frictional sliding. In *J. Phys. D: Appl. Phys.* 42 (21), p. 214016. DOI: 10.1088/0022-3727/42/21/214016.

Sawyer, W. Gregory; Wahl, Kathryn J. (2008): Accessing Inaccessible Interfaces. In Situ Approaches to Materials Tribology. In *MRS Bull.* 33 (12), pp. 1145–1150. DOI: 10.1557/mrs2008.244.

Schallamach, A. (1971): How does rubber slide? In *Wear* 17 (4), pp. 301–312. DOI: 10.1016/0043-1648(71)90033-0.

Schulze, Kyle D.; Bennett, Alex I.; Marshall, Samantha; Rowe, Kyle G.; Dunn, Alison C. (2016): Real Area of Contact in a Soft Transparent Interface by Particle Exclusion Microscopy. In *J. Tribol* 138 (4), p. 41404. DOI: 10.1115/1.4032822.

Sills, Scott; Vorvolakos, Katherine; Chaudhury, Manoj K.; Overney, René M. (2007): Molecular Origins of Elastomeric Friction. In Enrico Gnecco, E. Meyer (Eds.): Fundamentals of friction and wear, vol. 79. Berlin, New York: Springer (NanoScience and Technology), pp. 659–676.

Uchiyama, Y. (1985): Friction and surface deformation of rubber. In *Nippon Gomu Kyokashi (Japan)* 58, p. 319.

Viswanathan, Koushik; Mahato, Anirban; Yeung, Ho; Chandrasekar, Srinivasan (2017): Surface phenomena revealed by in situ imaging. Studies from adhesion, wear and cutting. In *Surf. Topogr.: Metrol. Prop.* 5 (1), p. 14002. DOI: 10.1088/2051-672X/aa612a.

Weiqiang, Wang; Shizhu, Wen (1994): In situ observation and study of the unlubricated wear process. In *Wear* 171 (1-2), pp. 19–23. DOI: 10.1016/0043-1648(94)90343-3.

Zeng, Hongbo (2013): Polymer adhesion, friction, and lubrication. Available online at http://lib.myilibrary.com/Open.aspx?id=450259.

Zhang, Si-Wei (2004): Tribology of elastomers. 1. ed. Amsterdam: Elsevier (Tribology and interface engineering series, 47). Available online at http://www.sciencedirect.com/science/publication?issn=15723364&volume=47.